Molecular Crystals and Liquid Crystals
Publication details, including instructions for authors and subscription information:
http://www.tandfonline.com/loi/gmcl20

Large Pentacene and Fullerene Crystals Having a Well-Defined Polygon

Takeshi Yamao [a], Takao Nakagawa [a], Keniji Ogino [a b], Norihiro Noguchi [a c] & Shu Hotta [a]

[a] Department of Macromolecular Science and Engineering, Kyoto Institute of Technology, Matsugasaki, Sakyo-ku, Kyoto, Japan

[b] Fukui Prefectural Institute of Public Health and Environmental Science, 39-4 Harame-cho, Fukui, 910-8551, Japan

[c] Kyoto Institute of Thin-Film Technology & Application, 418 Yodokizu-cho, Fushimi-ku, Kyoto, 613-0911, Japan

To cite this article: Takeshi Yamao, Takao Nakagawa, Keniji Ogino, Norihiro Noguchi & Shu Hotta (2013) Large Pentacene and Fullerene Crystals Having a Well-Defined Polygon, Molecular Crystals and Liquid Crystals, 581:1, 1-6

To link to this article: http://dx.doi.org/10.1080/15421406.2013.808126

Mol. Cryst. Liq. Cryst., Vol. 581: pp. 1–6, 2013

ISSN: 1542-1406 print/1563-5287 online
DOI: 10.1080/15421406.2013.808126

Taylor & Francis
Taylor & Francis Group

Large Pentacene and Fullerene Crystals Having a Well-Defined Polygon

TAKESHI YAMAO,* TAKAO NAKAGAWA, KENIJI OGINO,[1] NORIHIRO NOGUCHI,[2] AND SHU HOTTA

Department of Macromolecular Science and Engineering, Kyoto Institute of Technology, Matsugasaki, Sakyo-ku, Kyoto, Japan

We have been successful in growing well-defined polygon crystals of fullerene and pentacene in liquid and vapor phases, respectively. These crystals were grown directly or laminated on substrates, allowing us to carry out their detailed structural characterization. We estimated the crystal structure of fullerene crystals by comparing the results of microscope and X-ray diffraction (XRD) observations with the crystal structure of a solvate. We carried out spectroscopic and XRD measurements on the pentacene crystals. Combining density functional theory calculations with the polarizing microscope observation, we related the principal axes of refractive index to the crystal geometry of pentacene.

Keywords Crystal growth; pentacene; fullerene; organic photovoltaic cells; dielectric tensor

Introduction

Organic photovoltaic cells (OPVs) are attracting a lot of attention as an easily-fabricated solar energy conversion device. In most cases they consist of multilayered structures [1,2] or bulk heterojunctions (BHJs) [3]. In particular, the BHJs enabled a high power conversion efficiency up to ∼10% at laboratory level [4]. The relevant morphology made it possible to achieve effective charge separation, even though organic materials comprising the BHJs have a relatively small exciton diffusion length (∼10 nm). Such characteristics of the BHJs are based upon the morphology optimization of the phase-separated binary system. Instead, however, one often ignored the quantification and maximization of physical quantities and parameters such as an exciton diffusion length.

In contrast to disordered systems as typified by the BHJs, organic crystals indicate enhanced electrical and optical properties [5,6] because of the regular arrangement of the molecules. This is expected to be the case as well with the OPVs. In this context Herrmann et al. [7] observed that the spectroscopic characteristics differed greatly depending upon the

*Address correspondence to Takeshi Yamao, Department of Macromolecular Science and Engineering, Kyoto Institute of Technology, Matsugasaki, Sakyo-ku, Kyoto 606-8585, Japan. Tel.: +81-75-724-7780; Fax: +81-75-724-7800. E-mail: yamao@kit.ac.jp

[1]Present address: Fukui Prefectural Institute of Public Health and Environmental Science, 39-4 Harame-cho, Fukui 910-8551, Japan

[2]Present address: Kyoto Institute of Thin-Film Technology & Application, 418 Yodokizu-cho, Fushimi-ku, Kyoto 613-0911, Japan

morphologies (i.e. regioregular and regiorandom) of poly(3-hexylthiophene) and inferred that the former morphology seemed more suitable for PVs.

This prompted us to investigate the OPV materials of a high degree of order, especially crystals. Large enough crystals in firm contact with substrates should be needed to easily apply them to the PV devices. In the present studies we chose fullerene (C_{60}) and pentacene as the OPV materials and improved their crystal growth methods both in liquid phase [8] and vapor phase [9] to conform the crystals to the PV devices. As a result we have been successful in producing large crystals of a well-defined polygon. These crystals were grown directly on the substrate or easily laminated on the substrate. These polygon crystals allowed us to carry out their detailed structural characterization. As an initial approach we characterized these crystals via micrographs and X-ray diffraction (XRD) observations. We also related the principal axes of refractive index to the crystal geometry of pentacene. The crystallographic information such as the crystal axes and the principal axes is indispensable for achieving good performance of the OPVs because it is related to the carrier transport and the optical absorption.

Experiments

We used C_{60} and pentacene as purchased (from Ushio Chemix Corporation or Sigma-Aldrich Co. LLC.) without further purification. For C_{60} crystals, we adopted liquid phase growth method [8] because C_{60} was soluble in some organic solvents and high temperatures ($\sim$550°C) were needed for vapor phase growth [10]. By the liquid phase growth we directly grew the crystals on a substrate [8]. We used a mixture liquid of the C_{60} powder material and its saturated solution. We selected n-decane, monochlorobenzene, and 1,2,4-trichlorobenzene as the solvent. The substrate was closely attached on a thermal radiator and was immersed into the mixture liquid that was heated with an electrical heater. Because the substrate was cooled locally in the liquid, C_{60} was directly deposited onto the substrate through recrystallization. To adjust cooling efficiency by the difference in thermal conductivity of metals, we prepared a plate of brass, aluminum, or stainless steel for the radiator. The growth temperature and time were varied from 100 to 190°C and from 52 to 408 h, respectively.

In turn, we chose the vapor-phase method [9] for the crystal growth of pentacene because pentacene was degraded in the organic solution in the presence of light and air [11]. The growth apparatus mainly consisted of a thick glass tube of 25 mm in diameter and two band (source and growth) heaters that were placed side-by-side at the bottom of the glass tube. Another thin glass tube of 4 mm in diameter was used in the thick glass tube for a nitrogen gas flow. We set the temperatures of the source and growth heaters at 240–255 and 190°C, respectively. As an option, we choked the thick glass tube with silica wool to reduce nitrogen gas flow and to grow the pentacene crystals under a quasi-equilibrium condition [12]. After 6–37 hour growth we placed the crystals on a substrate. The XRD measurements were performed using the C_{60} and pentacene crystals that were grown (or placed) on an Si wafer substrate covered with an SiO_2 layer (300 nm in thickness) [8].

Thicknesses of both crystals were measured using a surface profiler [8]. We observed the size, shape, and polarized characteristic of the crystals with a NIKON ECLIPSE LV100POL microscope with a mercury lamp (wavelength: 294.5–812.5 nm). The polarizing directions of the polarizer (P) and the analyzer (A) were set parallel to the horizontal and vertical directions, respectively. Polarized absorbance measurements of a pentacene crystal (different from that for the XRD measurement) were carried out under the extinction

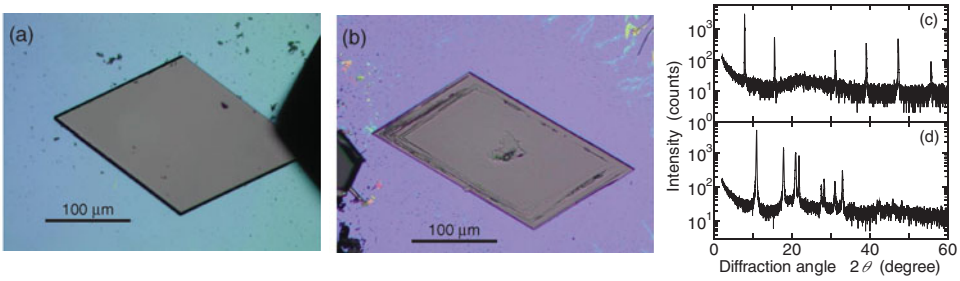

Figure 1. Micrographs of C_{60} crystals grown using (a) a brass radiator and (b) an aluminum radiator. The crystal was grown on an SiO_2/Si substrate in the liquid phase. We used 1,2,4-trichlorobenzene for the solvent. XRD patterns of (c) the C_{60} crystal of (a) and (d) the C_{60} powder.

position using the method similar to that described in the literature [13]. For this the crystal was laminated on a quartz glass substrate.

Using the atomic coordinates from the crystallographic data of pentacene [14], we calculated the dipole polarizability tensor [$\boldsymbol{\alpha}$] as a function of wavelength (400 to 800 nm). We performed the density functional theory (DFT) calculations using Gaussian 09 [15] program. We employed B3LYP and the Coulomb-attenuating method (CAM-B3LYP) [16] with the 6-31G(d) basis set.

Results and Discussion

We obtained parallelogram C_{60} crystals when we used the brass and aluminum radiators and 1,2,4-trichlorobenzene for the solvent. Figures 1(a) and (b) show micrographs of the C_{60} crystals. The short and long sides of the crystal in Fig. 1(a) [Fig. 1(b)] were 167 and 187 μm (138 and 224 μm), respectively. Their typical acute (obtuse) angle ranged 62.5–63.2° (116.8–117.3°). Figures 1(c) and (d) compare XRD patterns (θ-2θ scan) of the parallelogram crystal and the C_{60} powder (as purchased). Diffraction peaks in Fig. 1(d) correspond to those for the face-centered cubic (fcc) structure of pristine C_{60} [17]. In Fig. 1(c) a sharply resolved line at 7.85° is due to the first-order diffraction and higher-order lines up to the seventh order are well-resolved as well. The plane separation evaluated from these diffraction lines is $d = 11.60$ Å.

Among several crystal structures reported for solvated C_{60} crystals [18,19], the bromobenzene solvate belongs to the monoclinic system [18]. Its [110] and [1$\bar{1}$0] directions meet at an angle of 61.07°. The spacing between the *ab*-planes is 10.78 Å. By comparing our data with those in Ref. [18], we infer that the crystals in Figs. 1(a) and (b) have a related crystal structure. Nonetheless, we were unable to determine the orientation of the C_{60} crystal that gives the extinction and diagonal positions because of complete darkness in the viewing field of the microscope.

Figure 2(a) shows a nonpolarizing micrograph of a pentacene crystal. Figures 2(b) and (c) show polarizing micrographs taken under the extinction and diagonal positions of the crossed Nicols, respectively. The crystal orientation of Fig. 2(a) is identical to that of Fig. 2(b). The parallelogram crystals were ~200 to ~800 μm in side and ~300 to ~700 nm in thickness. The specific crystal in Figs. 2(a)–(c) was 704 μm and 774 μm in both the sides. The angle indicated by the white curved arrow in Fig. 2(a) was 74.3°. This angle is in agreement with 77.59° between the [110] and [$\bar{1}$10] directions estimated from the reported crystal structure [14]. Figure 2(d) shows an XRD pattern of the pentacene crystal

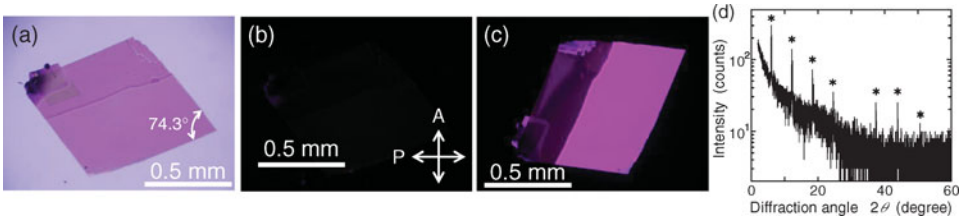

Figure 2. (a) Nonpolarizing micrograph of a pentacene crystal laminated on an SiO_2/Si substrate. The white curved arrow indicates an acute angle (74.3°) of the parallelogram crystal. Polarizing micrographs of the same crystal taken under (b) the extinction position and (c) the diagonal position of the crossed Nicols. In (b), A and P denote the polarization directions of the analyzer and polarizer, respectively. The orientation of the crystal of (a) is identical to that of (b). (d) XRD pattern of the same pentacene crystal. The asterisks indicate the first- and higher-order diffraction lines.

of Figs. 2(a)–(c). The first-order diffraction line is sharply resolved at 5.99° along with its higher-order diffraction lines up to the eighth order. From these lines we estimated the plane separation to be 14.38 Å. This separation is also in good agreement with that between the *ab*-planes (14.12 Å) estimated from the crystal structure [14]. This implies that the *ab*-plane is parallel to the substrate plane.

Figure 3(a) shows polarized absorbance spectra of the pentacene crystal. The spectra were measured along the P- and A-directions. Absorption edges for A- and P-directions arose at 708 and 643 nm, respectively. The spectra show that most of the visible light is absorbed and that the transmitted light mostly comes from that of ∼650 nm in wavelength.

Next, we relate the principal axes of refractive index of the crystal to the crystal geometry. To this end we calculated the dielectric tensor $[\boldsymbol{\varepsilon}]$ from $[\boldsymbol{\alpha}]$ [20] and estimated the impermeability tensor $[\boldsymbol{\eta}]$ ($\equiv [\boldsymbol{\varepsilon}]^{-1}$) [21]. Since the pentacene crystal is triclinic [14,22], the tensor $[\boldsymbol{\eta}]$ is a symmetric matrix with nonzero off-diagonal terms η_{ij}, where, i and j mean the x-, y-, or z-axis of the Cartesian coordinates. The tensor $[\boldsymbol{\eta}]$ represents the index

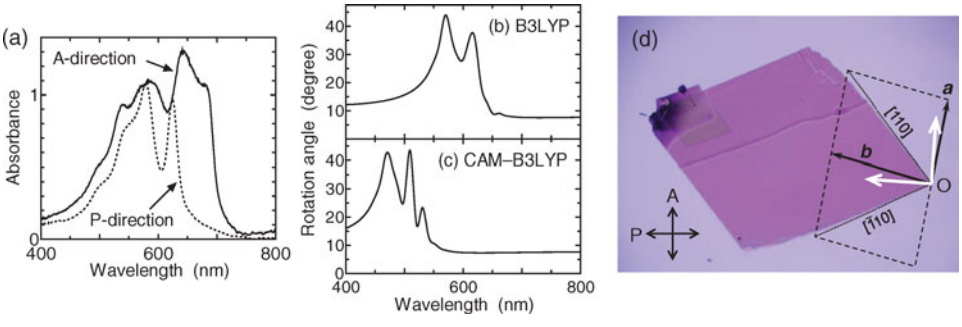

Figure 3. (a) Polarized absorbance spectra of a pentacene crystal. The measurements were carried out along the P- and A-directions with the crystal placed under the extinction position. Rotation angles of the principal axes computed using (b) B3LYP and (c) CAM-B3LYP. (d) Geometrical relationship between the crystal axes and the principal axes. The fundamental vectors $\boldsymbol{a}$ and $\boldsymbol{b}$ are indicated by black arrows. The dashed parallelograms indicate the unit cell of the pentacene crystal. The P- and A-directions represent the experimentally determined principal axes. White arrows show the directions of the computationally determined principal axes. Both the experimental and computational results agree within an error of 3.8°.

ellipsoid:

$$(x, y, z)[\boldsymbol{\eta}]\begin{pmatrix} x \\ y \\ z \end{pmatrix} = 1. \quad (1)$$

We set the *x*-axis to coincide with the *a*-axis with the *xy*-plane paralleling the *ab*-plane. The angle between the *y*- and *b*-axes was chosen as an acute angle. Setting $z = 0$ in Eq. (1) gives a bilinear form with respect to the coordinates *x* and *y*. Diagonalizing the resulting tensor (a 2×2 matrix), we determined the directions of the principal axes of an *ellipse* on the *xy*-plane (substrate plane). Note that the ellipse is obtained by intercepting the above-mentioned ellipsoid at the plane of $z = 0$. Henceforth the principal axis is relevant to that ellipse.

Thus we estimated the rotation angle of the principal axes relative to the original *xy*-coordinate system. Figures 3(b) and (c) represent the computational data. In Fig. 3(b) [Fig. 3(c)] the rotation angle was estimated to be ∼7.6° [∼7.3–7.7°] at wavelengths longer than 700 nm [600 nm]. Comparing Fig. 3(a) with Figs. 3(b) and (c) we conclude that the averaged rotation angle 7.6° is a most likely estimation by computation. In Fig. 3(d) white arrows indicate the principal axes determined by this rotation angle. The fundamental vectors ***a*** and ***b*** are chosen from Ref. [14]. Dashed lines represent the relevant unit cells. The angle 74.3° [Fig. 2(a)] of our result is pretty close to 77.59° between the [110] and [$\bar{1}$10] directions [14]. The bisectors of these angles are chosen to be identical. We assume that the principal axes should be parallel to the P- and A-directions [23]. In Fig. 3(d) the P- and A-directions are rotated 11.4° relative to the *xy*-coordinate system. Consequently, both the experimental and computational results agree within an error of 3.8°.

Conclusions

We have grown well-defined polygon crystals of C_{60} and pentacene in the liquid and vapor phases, respectively. With these crystals, we have performed the precise structural characterizations. Using the parallelogram C_{60} crystals, we compared their specific angles and the plane separation evaluated from the XRD pattern with the crystal structure of the bromobenzene solvate and inferred that the present C_{60} crystals had the related structure. As for the pentacene crystal, we combined the crystal geometry under the extinction position of the polarizing micrograph with the principal axes determined from the DFT calculation. As a result, we were able to relate the crystal orientation to these principal axes.

The present polygon thin crystals can be grown directly on the substrate or easily laminated on the substrate. Moreover, these crystals are large enough to fabricate the OPV devices on them.

Acknowledgments

We thank Dr. Jenny Clark for her helpful discussions and suggestions. This work was supported by Grants-in-Aid for Science Research (B) and (C) and Challenging Exploratory Research from the Ministry of Education, Culture, Sports, Science and Technology, Japan. This work was also supported in part by the Murata Science Foundation.

References

[1] Tang, C. W. (1986). *Appl. Phys. Lett.*, *48*, 183.
[2] Hiramoto, M., Fujiwara, H., & Yokoyama, M. (1992). *J. Appl. Phys.*, *72*, 3781.

[3] Yu, G., Gao, J., Hummelen, J. C., Wudl, F., & Heeger, A. J. (1995). *Science*, *270*, 1789.
[4] Service, R. F. (2011). *Science*, *332*, 293.
[5] Ichikawa, M., Hibino, R., Inoue, M., Haritani, T., Hotta, S., Araki, K., Koyama, T., & Taniguchi, Y. (2005). *Adv. Mater.*, *17*, 2073.
[6] Yamagishi, M., Takeya, J., Tominari, Y., Nakazawa, Y., Kuroda, T., Ikehata, S., Uno, M., Nishikawa, T., & Kawase, T. (2007). *Appl. Phys. Lett.*, *90*, 182117.
[7] Herrmann, D., Niesar, S., Scharsich, C., Köhler, A., Stutzmann, M., & Riedle, E. (2011). *J. Am. Chem. Soc.*, *133*, 18220.
[8] Yamao, T., Miki, T., Akagami, H., Nishimoto, Y., Ota, S., & Hotta, S. (2007). *Chem. Mater.*, *19*, 3748.
[9] Yamao, T., Ota, S., Miki, T., Hotta, S., & Azumi, R. (2008). *Thin Solid Films*, *516*, 2527.
[10] Matsuura, S., Ishiguro, T., Kikuchi, K., & Achiba, Y. (1995). *Phys. Rev. B*, *51*, 10217.
[11] Maliakal, A., Raghavachari, K., Katz, H., Chandross, E., & Siegrist, T. (2004). *Chem. Mater.*, *16*, 4980.
[12] Ichikawa, M., Hibino, R., Inoue, M., Haritani, T., Hotta, S., Koyama, T., & Taniguchi, Y. (2003). *Adv. Mater.*, *15*, 213.
[13] Yamao, T., Taniguchi, Y., Yamamoto, K., Miki, T., Ota, S., Hotta, S., Goto, M., & Azumi, R. (2007). *Jpn. J. Appl. Phys.*, *46*, 7478.
[14] Siegrist, T., Kloc, C., Schön, J. H., Batlogg, B., Haddon, R. C., Berg, S., & Thomas, G. A. (2001). *Angew. Chem., Int. Ed.*, *40*, 1732.
[15] Gaussian 09 Revision B.01 (Gaussian, Inc., Wallingford, CT, 2009).
[16] Limacher, P. A., Mikkelsen, K. V., & Lüthi, H. P. (2009). *J. Chem. Phys.*, *130*, 194114.
[17] Iwasa, Y., Arima, T., Fleming, R. M., Siegrist, T., Zhou, O., Haddon, R. C., Rothberg, L. J., Lyons, K. B., Carter Jr., H. L., Hebard, A. F., Tycko, R., Dabbagh, G., Krajewski, J. J., Thomas, G. A., & Yagi, T. (1994). *Science*, *264*, 1570.
[18] Korobov, M. V., Mirakian, A. L., Avramenko, N. V., Valeev, E. F., Neretin, I. S., Slovokhotov, Y. L., Smith, A. L., Olofsson, G., & Ruoff, R. S. (1998). *J. Phys. Chem. B*, *102*, 3712.
[19] Korobov, M. V., Stukalin, E. B., Mirakyan, A. L., Neretin, I. S., Slovokhotov, Y. L., Dzyabchenko, A. V., Ancharov, A. I., & Tolochko, B. P. (2003). *Carbon*, *41*, 2743.
[20] Smith, F. G., King, T. A., & Wilkins, D. (2007). *Optics and Photonics: An Introduction*, John Wiley & Sons, Ltd, Chichester, England.
[21] Boyd, R. W. (2008). *Nonlinear Optics*, Academic Press, Burlington, U. S. A.
[22] Mattheus, C. C., Dros, A. B., Baas, J., Meetsma, A., de Boer, J. L., & Palstra, T. T. M. (2001). *Acta Crystallogr., Sect. C: Cryst. Struct. Commun.*, *57*, 939.
[23] Scharf, T. (2006). *Polarized Light in Liquid Crystals and Polymers*, John Wiley & Sons, Inc., Hoboken, New Jersey, U. S. A.